Journal of Physics B: Atomic, Molecular and Optical Physics

PAPER • **OPEN ACCESS**

Synthetic spectra of BeH, BeD and BeT for emission modeling in JET plasmas

To cite this article: D Darby-Lewis *et al* 2018 *J. Phys. B: At. Mol. Opt. Phys.* **51** 185701

OPEN ACCESS
IOP Publishing
Journal of Physics B: Atomic, Molecular and Optical Physics
J. Phys. B: At. Mol. Opt. Phys. **51** (2018) 185701 (12pp)
https://doi.org/10.1088/1361-6455/aad6d0

Synthetic spectra of BeH, BeD and BeT for emission modeling in JET plasmas

D Darby-Lewis[1], J Tennyson[1,5], K D Lawson[2], S N Yurchenko[1], M F Stamp[2], A Shaw[2], S Brezinsek[3] and JET Contributors[4]

[1] Department of Physics & Astronomy, University College London, Gower St.,London, WC1E 6BT, United Kingdom
[2] UKAEA/CCFE, Culham Science Centre, Abingdon, OX14 3DB, United Kingdom
[3] Institut für Energie und Klimaforschung—Plasmaphysik Forschungszentrum Jülich GmbH Wilhelm-Johnen-Straße, D-52428 Jülich, Germany

E-mail: daniel.darby.11@ucl.ac.uk, j.tennyson@ucl.ac.uk and kerry.lawson@ukaea.uk

Received 28 March 2018, revised 26 June 2018
Accepted for publication 30 July 2018
Published 24 August 2018

Abstract

A theoretical model for isotopologues of beryllium monohydride, BeH, BeD and BeT, A $^2\Pi$ to X $^2\Sigma^+$ visible and X $^2\Sigma^+$ to X $^2\Sigma^+$ infrared rovibronic spectra is presented. The MARVEL procedure is used to compute empirical rovibronic energy levels for BeH, BeD and BeT, using experimental transition data for the X $^2\Sigma^+$, A $^2\Pi$, and C $^2\Sigma^+$ states. The energy levels from these calculations are then used in the program Duo to produce a potential energy curve for the ground state, X $^2\Sigma$, and to fit an improved potential energy curve for the first excited state, A $^2\Pi$, including a spin–orbit coupling term, a Λ-doubling state to state (A–X states) coupling term, and Born–Oppenheimer breakdown terms for both curves. These, along with a previously computed *ab initio* dipole curve for the X and A states are used to generate vibrational-rotational wavefunctions, transition energies and A-values. From the transition energies and Einstein coefficients, accurate assigned synthetic spectra for BeH and its isotopologues are obtained at given rotational and vibrational temperatures. The BeH spectrum is compared with a high resolution hollow-cathode lamp spectrum and the BeD spectrum with high resolution spectra from JET giving effective vibrational and rotational temperatures. Full A–X and X–X line lists are given for BeH, BeD and BeT and provided as supplementary data on the ExoMol website.

Supplementary material for this article is available online

Keywords: Fusion, emission spectrum, beryllium monohydride

(Some figures may appear in colour only in the online journal)

1. Introduction

In order to predict the erosion, migration and re-deposition of the Be first wall in fusion devices such as JET, and in the future ITER, and in view of impurity production and lifetime of components, an understanding of the release and transport of Be is an essential requirement. BeT is also important for modeling tritium retention in beryllium containing fusion devices. BeD_X release was shown to contribute more than 50% to the total erosion in certain cases in JET D plasmas in a limiter configuration deduced from BeD emission spectra (Brezinsek *et al* 2014). Detailed studies of molecular spectra (Duxbury *et al* 1998), such as those for BeH, BeD, and BeT A–X bands can provide valuable input to codes used for erosion modeling such as ERO (Borodin *et al* 2011, Lasa *et al* 2018). To this end, we develop a full spectroscopic model for BeH, BeD and BeT X $^2\Sigma^+$ and A $^2\Pi$ states based on explicit potential energy curves (PECs), spin–orbit (LS)

[4] See the author list of 'Litaudon *et al* 2017 *Nucl. Fusion* **57** 102001'.
[5] Author to whom any correspondence should be addressed.

and Λ doubling (L^+) couplings, Born–Oppenheimer breakdown (BOB) terms, and *ab initio* dipole curves. The PECs, couplings, and BOB terms are derived using accurate experimentally recorded transition frequencies. A previous PEC fitting for the X state by Le Roy *et al* (2006) has been improved upon by Dattani (2015), and further refined in this work by fitting procedures involving the X–A state transitions. The A state PEC was previously studied by Le Roy *et al* (2006) and is also improved upon here. Accurate *ab initio* calculations for the X state were performed by Koput (2011). The fitting in Duo (Yurchenko *et al* 2018) results in a full set of accurate transitions for BeH, BeD, and BeT from a single set of PECs, couplings, and BOB terms (Le Roy 2017). These data are used to determine temperatures in the experimental spectra. This method of using variational nuclear motion calculations with BOB terms to link isotopologue data differs from the methods based on perturbation theory generally employed up until now, see Duxbury *et al* (1998) and Hornkohl *et al* (1991). These older methods use spectroscopic constants to calculate energies but cannot join isotopologue data and thus do not provide predictions for yet-to-be observed isotopologues. Our approach is similar in spirit to that adopted by Parigger *et al* (2015) to model laser ablation and by McGuire *et al* (2016) to model plasma ablation.

Our line lists for BeH, BeD and BeT improve on those of Yadin *et al* (2012) produced as part of the ExoMol project (Tennyson and Yurchenko 2012) both in having greater range and improved accuracy in the transition frequencies. The present paper aims to give a more accurate fit to the spectrum of the BeD A–X transition than was achieved by Duxbury *et al* (1998) and Björkas *et al* (2013) by using more accurate transition data and allowing separated treatment of vibrational and rotational temperatures. The use of different rotational and vibrational temperatures, which implies there is no local thermodynamic equilibrium (non-LTE), is expected to lead to a more accurate description of the experimental spectrum.

We compare theoretically produced synthesized spectra to new experimental BeD spectra recorded on JET and BeH spectra recorded in Be hollow-cathode discharges in Forschungszentrum Jülich. Both of these spectra were recorded employing spectrometers with high spectral resolution in the visible range, sufficient to resolve the rotational lines.

2. Theory

There are four main steps in generating assigned synthetic spectra fitted with rotational and vibrational temperatures. Experimental transitions are inverted to give vibronic energy levels using the online implementation of MARVEL (measured active rotation vibration energy levels). These are then used in Duo to fit PECs which can accurately reproduce all the empirical energy levels. Empirical energy levels belonging to the X $^2\Sigma^+$, A $^2\Pi$ and C $^2\Sigma^+$ electronic states are provided by our MARVEL treatment, although PECs were fitted only for the X and A states. This is because of a lack of transition data for the C state, which in any case does not give rise to a significant feature in the JET emission spectrum. To date, the molecular spectrum is dominated by the A–X band. Duo uses an *ab initio* X state to A state transition dipole (Pitarch-Ruiz *et al* 2008) to produce Einstein A-coefficients for the observed X to A transitions. The output from Duo contains all transitions between states within a given wavenumber range (parameter in the Duo input, see supplementary data available online at stacks.iop.org/JPB/51/185701/mmedia) and all the Einstein A-coefficients associated with those energy levels. These are used by ExoCross to generate synthetic spectra with varying rotational and vibrational temperatures. These spectra are compared to experimental spectra to obtain a metric for the fit. The flowchart in figure 1 illustrates the links between the steps of this process, each step is presented in detail below.

2.1. MARVEL

MARVEL (Furtenbacher *et al* 2007, Furtenbacher and Császár 2012) is a program with an online user interface which takes highly accurate experimental transition energies and calculates spectroscopic networks of energy levels. For BeH, BeD and BeT we used transitions involving X $^2\Sigma^+$, A $^2\Pi$ and C $^2\Sigma^+$, with assigned quantum numbers taken from the literature (Shayesteh *et al* 2003, Le Roy *et al* 2006). In particular Le Roy *et al* (2006) give transition data compiled from many sources including Shayesteh *et al* (2003), Colin *et al* (1983), Focsa *et al* (1998) and De Greef and Colin (1974).

Table 1 shows the transition data sources used for input to MARVEL. Comments on individual sources are as follows:

[H1] Le Roy *et al* (2006) contains A–X transitions $\Delta v = 0$ up to $v'' = 6$, $\Delta v = +1$ up to $v'' = 6$ and some transitions for C–X with $v'' = 0$–2 and $v' = 6$–10.
[H2] Shayesteh *et al* (2003) infrared, rovibrational transitions, were duplicated for $\Sigma = \pm 0.5$ giving 314 valid transitions.
[D1] Le Roy *et al* (2006) contains A–X transitions $\Delta v = 0$ up to $v'' = 6$, $\Delta v = +1$ up to $v'' = 5$ and some transitions for C–X with $v'' = 0$ and $v' = 8$–12.
[D2] Shayesteh *et al* (2003) infrared, rovibrational transitions, were duplicated for $\Sigma = \pm 0.5$ giving 328 valid transitions.
[T1] Le Roy *et al* (2006) contains only A–X transitions $\Delta v = 0$.

A small portion of the MARVEL input file for BeH is shown in table 2 where the column format is explained. The number of quantum numbers used for assignment here is 5. The thresholds for changing uncertainties and for deletion were both set to 3. The full files are given in the supplementary data.

These transitions are run through the program and various unlinked spectroscopic networks of energy levels are generated. Separate networks can be joined with 'linking' transitions, e.g. joining the degenerate spin up and spin down states of the ground state with a 'transition' of zero energy from one degenerate state to another. The result of this process is to give a large set of accurate energy levels with quantum number assignments. For BeH and BeD the infrared data of Shayesteh *et al* (2003) brings together separate

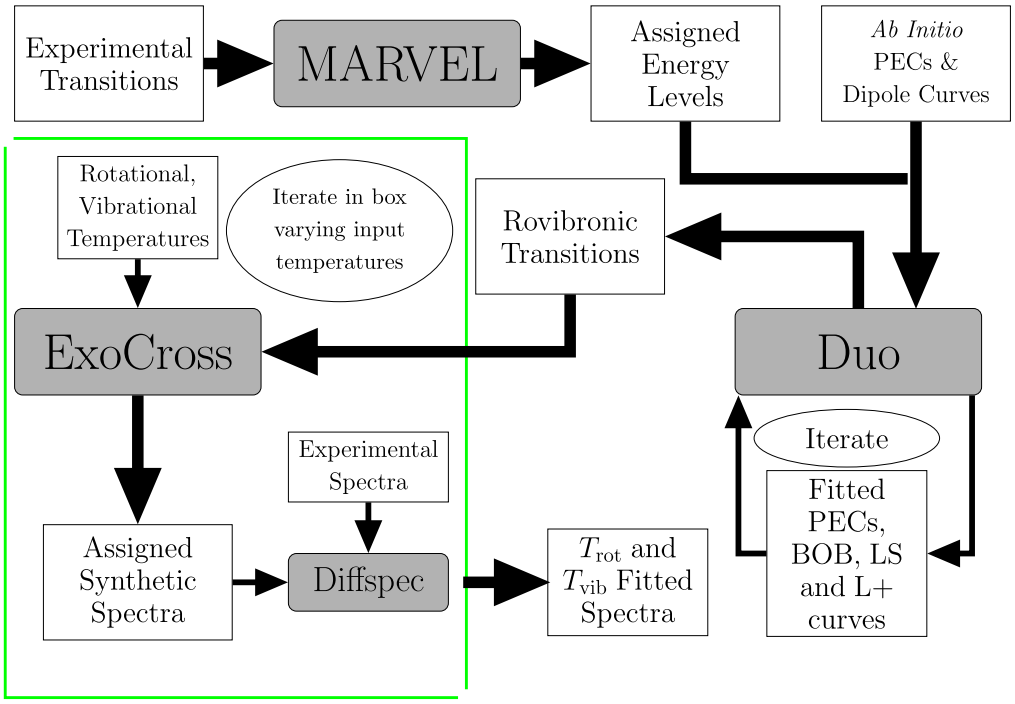

Figure 1. Flow diagram showing the production of high accuracy synthetic spectra, starting in the top left corner with collated experimental transitions and resulting in, bottom center, synthetic spectra with the best fit rotational and vibrational temperatures.

Table 1. Input transitions for MARVEL online. *See text for discussion on the comments.

Isotope	Tag	Range (cm^{-1})	States	Transitions	Largest network	Comments*
BeH						
	Le Roy *et al* (2006)	15 132–20 822	A–X, C–X	1887	1264	[H1]
	Shayesteh *et al* (2003)	1802–2239	X–X	160		[H2]
BeD						
	Le Roy *et al* (2006)	15 164–20 619	A–X, C–X	2276	1495	[D1]
	Shayesteh *et al* (2003)	1240–1680	X–X	167		[D2]
BeT						
	Le Roy *et al* (2006)	19 824–20 424	A–X, $\Delta v = 0$ only.	524	215	[T1]

vibrational networks. This results in two large networks separated along the quantum number Σ, where $\Sigma = -0.5$ for one network and $\Sigma = 0.5$ for the other. These two networks are joined with a linking transition with a 'magic' wavenumber, between states with opposing spin, as shown for BeH by the transition labeled MAGIC.001 in table 2. This magic transition is an artificial transition calculated from empirical, effective Hamiltonian energy levels belonging to separate networks. The frequency of the magic transition is calculated to produce degeneracy between the states with differing spin at low J.

The 'good' quantum numbers in this application are the total rotational quantum number (J) and total parity (+ or −). Quantum numbers of operators not strictly conserved in this application can still be used in state assignment. They are electronic state (X $^2\Sigma^+$, A $^2\Pi$ or C $^2\Sigma^+$), vibrational quantum number (v), nuclear rotational angular momentum (N), projection of total spin angular momentum (Σ), projection of total orbital angular momentum (Λ), and the projection of total electronic angular momentum $\Omega = \Lambda + \Sigma$. This places our representation in Hund's case b (Huber and Herzberg 1979, Bernath 2005). Figure 2 shows the rovibrational energy levels of the largest component network for BeH, BeD and BeT. The almost straight lines with isotopologue-dependent gradients are vibrational bands and the gradients depend on the rotational constants ($\propto 1/$reduced mass). Since the electronic states being represented here are doublets each point for an energy level shown in this figure actually corresponds to two spin degenerate states.

2.2. Duo

Duo (Yurchenko *et al* 2016) is a fully-coupled rovibronic nuclear motion code which generates rovibronic energy levels and wavefunctions for diatomic molecules from PECs, couplings between PECs, and Born–Oppenheimer correction terms This program contains an iterative fitting procedure

Table 2. Table of MARVEL input transitions for BeH with column labels and explanations.

1	2	3	4	5	6	7	8	9	10	11	12	13
$\tilde{\nu}$	$\Delta\tilde{\nu}$	State′	v'	$\left(J'+\frac{1}{2}\right)$	P'	Σ'	State″	v'	$\left(J''+\frac{1}{2}\right)$	P''	Σ''	ID
20.3282	0.001	1	0	1	−	−0.5	1	0	1	+	0.5	MAGIC.001
15 132.42	0.1	3	0	13	+	0.5	1	9	14	−	0.5	LeRoy.00001
15 204.53	0.1	3	0	12	−	0.5	1	9	13	+	0.5	LeRoy.00002
15 224.66	0.1	3	0	22	−	0.5	1	8	23	+	0.5	LeRoy.00003
15 273.77	0.2	3	0	11	+	0.5	1	9	12	−	0.5	LeRoy.00004
15 335.3	0.1	3	0	21	+	0.5	1	8	22	−	0.5	LeRoy.00005
15 339.62	0.1	3	0	10	−	0.5	1	9	11	+	0.5	LeRoy.00006
15 401.44	0.1	3	0	9	+	0.5	1	9	10	−	0.5	LeRoy.00007
15 433.71	0.1	3	0	13	+	0.5	1	9	12	−	0.5	LeRoy.00008
15 458.91	0.1	3	0	8	−	0.5	1	9	9	+	0.5	LeRoy.00009
15 485.93	0.1	3	0	12	−	0.5	1	9	11	+	0.5	LeRoy.00010

Column	Notation	
1	$\tilde{\nu}$	Transition frequency (cm^{-1})
2	$\Delta\tilde{\nu}$	Estimated uncertainty in transition frequency (cm^{-1})
3	State′	Initial electronic state, 1 = X $^2\Sigma^+$, 2 = A $^2\Pi$, 3 = C $^2\Sigma^+$
4	v'	Initial vibrational quantum number
5	$\left(J'+\frac{1}{2}\right)$	Initial total angular momentum quantum number plus 0.5
6	P'	Initial parity quantum number
7	Σ'	Initial electron angular momentum quantum number
8	State″	Final electronic state, 1 = X $^2\Sigma^+$, 2 = A $^2\Pi$, 3 = C $^2\Sigma^+$
9	v''	Final vibrational quantum number
10	$\left(J''+\frac{1}{2}\right)$	Final total angular momentum quantum number plus 0.5
11	P''	Final parity quantum number
12	Σ''	Final electron angular momentum quantum number
13	ID	Unique ID for transition with source label and counting number

where PECs and other terms can be fitted to experimental data. In this way the potential form of the ground state PEC, a Morse long range type potential (Le Roy *et al* 2011) as given by Pitarch-Ruiz *et al* (2008), is refitted using energy levels output from MARVEL. A new PEC, of the extended Morse oscillator type, is fitted to the A $^2\Pi$ excited state using energy levels from output from MARVEL. The A $^2\Pi$ PEC is modified by the addition of an LS coupling curve and an X to A state L^+ (Λ-doubling) coupling curve. Both the ground and excited state PECs are modified by the fitting of adiabatic and non-adiabatic BOB curves (Le Roy 2017) using the BeD and BeT isotopologue energy level data from MARVEL. Using BOB correction terms makes these data applicable to all isotopologues of BeH. This allows data from all three isotopologues to improve the fit from the same set of PECs and coupling terms. The fitting of BOB terms is achieved using an iterative process in Duo. The non-adiabatic BOB term is an additive correction to the PEC which has an increasing effect with increasing isotope mass (from zero effect on H, to $\frac{1}{2}$ on D, to $\frac{2}{3}$ on T). However due to the limited data for BeT it is initially fitted to the BeD data and adjusted iteratively for BeT. The adiabatic BOB term is a multiplicative factor applied to the centrifugal potential and has greatest effect on the lighter isotope; it is therefore initially fitted to BeH and adjusted to model BeD and BeT. When a suitable fit is produced for both states using the available energy levels from MARVEL, Duo allows fittings to be performed using the transitions. This allows a larger set of data to be used in the fitting routine, as some of the energy levels output by MARVEL cannot be connected to the main spectroscopic network.

Tables 3 and 4 show some of the energy levels generated by Duo for BeH, BeD and BeT for both the X and A states, they are each followed by the energies from MARVEL used in the fitting for those levels. As shown earlier, in table 1, only the $v = 0$ component of BeT joins the main network of transitions, as there are no measured $\Delta v \neq 0$ transitions for BeT. Overall the root mean square of the fit for each isotopologue is: BeH, 0.542 cm^{-1}; BeD, 0.614 cm^{-1}; BeT, 0.384 cm^{-1}; for low-lying states much higher accuracies were achieved. PECs modified and fit by Duo for the X and A states of BeH, BeD and BeT are shown in figure 3. The zero point energy of these curves are: 1022.0292 cm^{-1} for BeH; 742.7911 cm^{-1} for BeD; 626.2844 cm^{-1} for BeT. The Duo input containing the PECs, couplings and BOB terms is given for BeH, BeD and BeT in the supplementary data. Predissociation is not included in this model.

Fully fitted PECs, couplings and BOB terms are used in conjunction with an *ab initio* transition dipole curve (Pitarch-Ruiz *et al* 2008) for the A to X state to generate Einstein A-coefficients for the rovibronic transitions. Duo

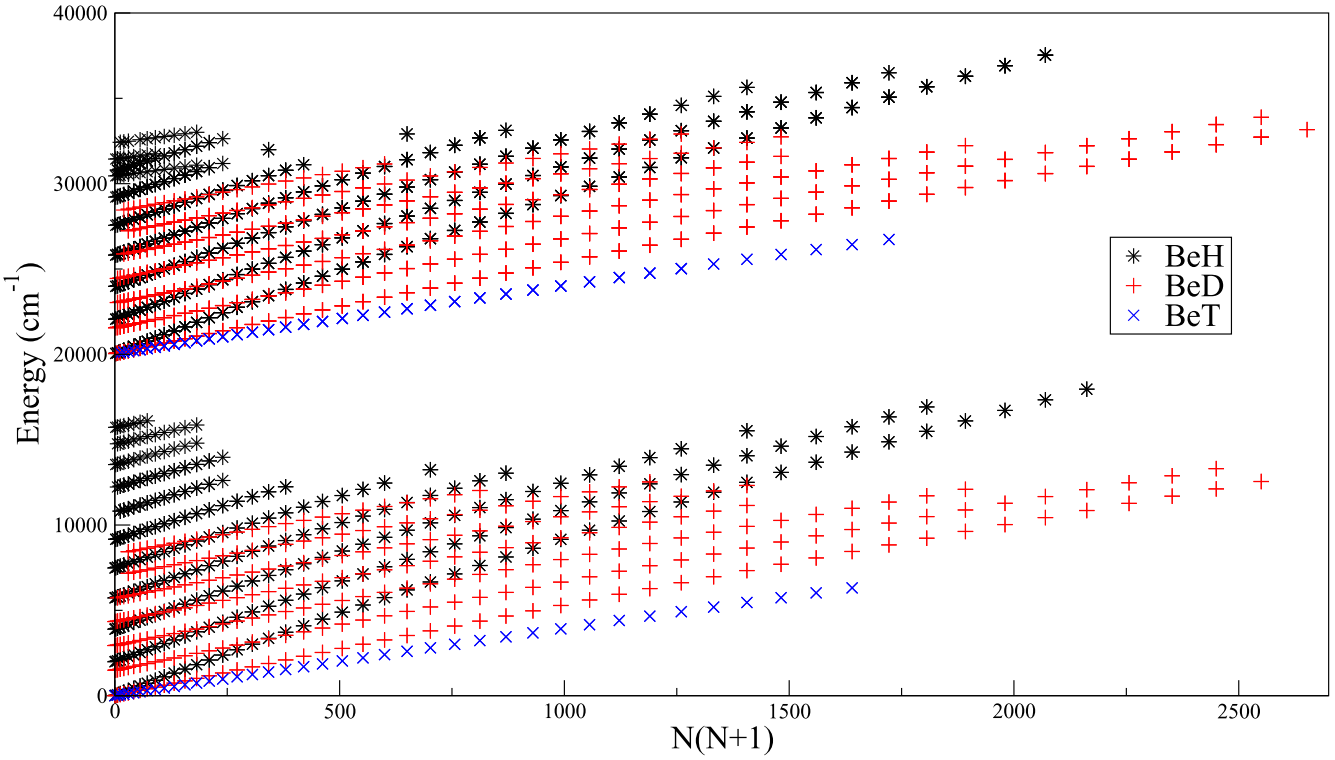

Figure 2. Output rovibronic energy levels from MARVEL for the largest spectroscopic networks of BeH, BeD, and BeT, against nuclear rotational quantum number, N, times nuclear rotational quantum number plus one. The rovibrational states of X $^2\Sigma^+$ are the lower set and the A $^2\Pi$ rovibrational states start at 20 000 cm^{-1}. Each of the energy levels represented here actually corresponds to two spin degenerate energy levels as both the X and the A states are doublets.

outputs two files for the line list of each isotopologue, one containing the list of the states involved in the transitions and the other being a list of the transitions between states and their A-values; this corresponds to the format of the ExoMol database (Tennyson *et al* 2013, 2016). The start of the states file and the start of the trans file for BeH are shown respectively in tables 5 and 6 followed by an explanation of their column formats. The entirety of the line list states and trans files for each isotopologue can be found in the supplementary data and on the ExoMol website (www.exomol.com).

3. Experiment

3.1. BeH hollow-cathode discharge spectrum

Experimental BeH spectra were recorded using a high resolution visible spectrometer, in cross-dispersion arrangement (grating and prism) covering the spectral range between 373 and 680 nm simultaneously in more than 50 orders with an almost constant resolving power of 1/DL ≈200 00, as show by Brezinsek *et al* (2008). The spectral source was a beryllium hollow-cathode discharge lamp with a neon/hydrogen mixture as a working gas. Inside the lamp, the metallic Be target plate is biased, resulting in it being bombarded by the impurity ions with Be being sputtered, either as Be or BeH_X. The current and voltage can be varied changing the plasma characteristics as well as the impact energy of the impinging ions. The released Be or BeH is then excited by electron impact leading to the emission of Be I, Be II as well as BeH light. Figure 4 shows the experimental spectra of the BeH A–X transition as well as the best-fitting simulated spectrum.

3.2. BeD JET edge emission spectra

An experimental BeD A–X spectrum was measured in four consecutive JET 2.4 T, 2.0 MA discharges with comparable conditions during the limiter phase of the pulse at 4.7–5.1 s. During this time, the plasma was limited by the inner poloidal limiter and BeD radiation was emitted from this region. It was recorded with a high resolution visible spectrometer (KS3), which had a Czerny–Turner arrangement and directly observed the low density edge plasma close to the inner poloidal limiter. The spectral wavelength range of the spectrometer does not cover the whole spectrum and so four consecutive discharges were chosen to form a joined image, see figure 5, with comparable plasma conditions as well as assumed comparable rovibrational populations.

4. Spectral analysis

The final step in generating an assigned synthetic spectra is performed using a program called ExoCross (Yurchenko *et al* 2018). ExoCross produces cross-sections for the absorption or emission of photons by molecules. It uses rotational, vibrational and electronic temperatures to produce a statistical (Boltzmann) population model. The equation for

Table 3. Comparison of excitation energies as a function of vibrational quanta, v, computed with Duo and obtained by MARVEL for: BeH and BeD X $^2\Sigma^+$ at $J = 0.5$, $\Omega = 0.5$, parity $= +$; BeT X $^2\Sigma^+$ at $J = 2.5$, $\Omega = 0.5$, parity $= -$.

v	X $^2\Sigma$					
	BeH		BeD		BeT	
	Duo	MARVEL	Duo	MARVEL	Duo	MARVEL
0	0	0	0	0	49.2756	50.3
1	1986.3054	1986.4169	1488.4401	1488.8472	1323.9046	
2	3896.8004	3896.8707	2935.6045	2936.1953	2568.5846	
3	5729.2711	5729.2613	4340.7423	4341.3802	3782.8768	
4	7480.4545	7480.4219	5702.8860		4966.2478	
5	9145.4221		7020.7372		6118.0189	
6	10 716.6777		8292.5346		7237.3131	
7	12 182.7098		9515.8791		8322.9914	
8	13 525.5493		10 687.4899		9373.5704	
9	14 716.2767		11 802.8549		10 387.1133	
10	15 705.6510		12 855.7188		11 361.0802	
11	16 402.4285		13 837.299		12 292.1239	
12	16 664.9980		14 735.0110		13 175.8010	
13			15 530.2285		14 006.1479	
14			16 194.0499		14 775.0274	
15			16 679.3277		15 471.0599	
16			16 918.4202		16 077.7733	
17			16 956.8145		16 570.2919	
18					16 910.3608	
19					17 056.2519	
20					17 076.5405	

Table 4. Comparison of excitation energies as a function of vibrational quanta, v, computed with Duo and obtained by MARVEL for: BeH and BeD A $^2\Pi^+$ at $J = 1.5$, $\Omega = 0.5$, parity $= +$; BeT A Π^+ at $J = 2.5$, $\Omega = 0.5$, parity $= -$.

v	A $^2\Pi$					
	BeH		BeD		BeT	
	Duo	MARVEL	Duo	MARVEL	Duo	MARVEL
0	20 050.8587	20 092.2658	20 048.3803	20 071.3872	20 089.3230	20 090.7
1	22 056.7376	22 097.0590	21 552.7700	21 575.8314	21 378.1542	
2	23 978.5785	24 017.3355	23 011.6534	23 034.2030	22 634.0613	
3	25 813.4908	25 850.6970	24 423.8044	24 445.6549	23 856.2579	
4	27 558.2734	27 594.5151	25 788.0151		25 043.9940	
5	29 208.9935	29 243.2969	27 102.9758		26 196.4966	
6	30 760.6586	30 793.4022	28 367.1779		27 312.9196	
7	32 206.9278		29 578.8347		28 392.3027	
8	33 539.8057		30 735.8129		29 433.5357	
9	34 749.2511		31 835.5682		30 435.3273	
10	35 822.6125		32 875.0780		31 396.1765	
11	36 743.7529		33 850.7620		32 314.3426	
12	37 491.6119		34 758.3833		33 187.8099	
13	38 037.6829		35 592.9147		34 014.2541	
14	38 341.2611		36 348.3556		34 790.9884	
15			37 017.4704		35 514.9038	
16			37 591.4032		36 182.3870	
17			38 059.0891		36 789.2084	
18			38 406.3136		37 330.3688	
19			38 614.1568		37 799.8866	
20					38 190.4670	
21					38 493.0018	
22					38 695.7499	
23					38 779.4876	

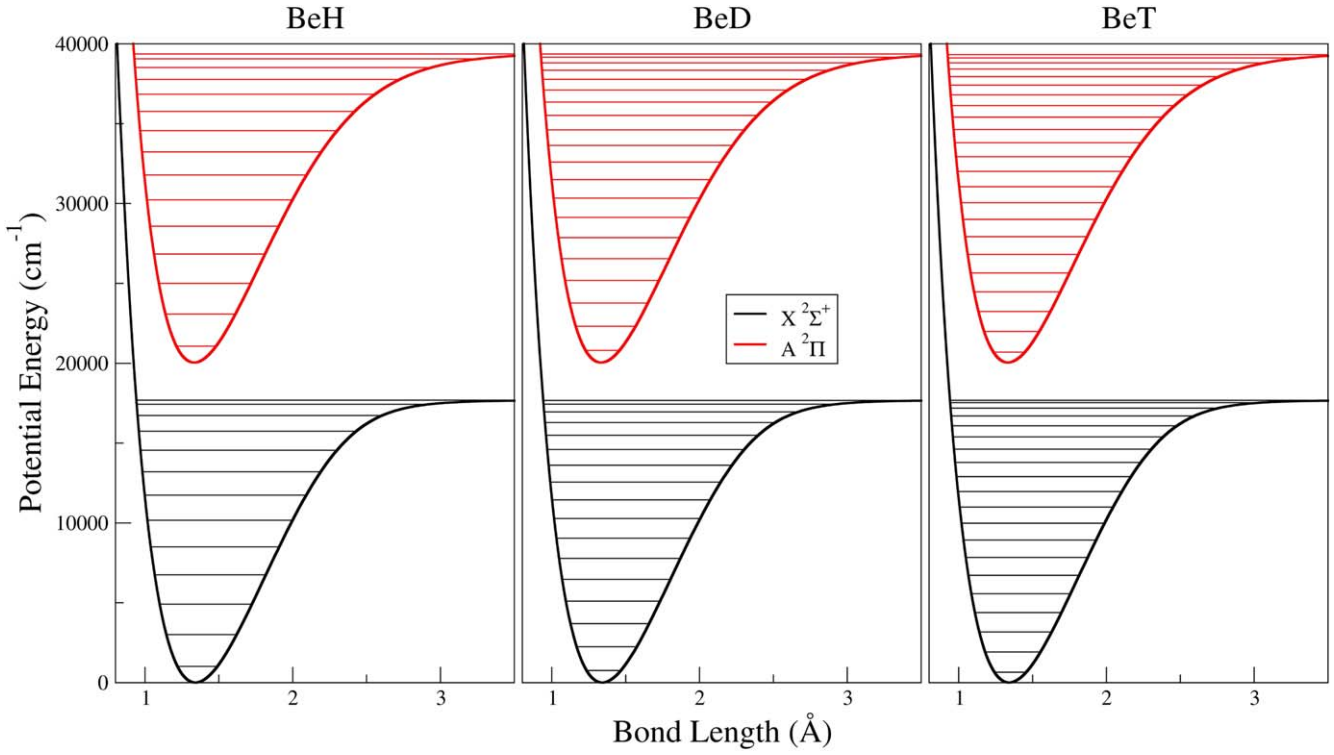

Figure 3. Fitted PECs for the X $^2\Sigma^+$ state and the A $^2\Pi$ state with vibrational energies at $J = 0.5$ for BeH, BeD, and BeT.

the population of a state: $P_{e,v,J}$ where e = electronic state, v = vibrational quanta, and J = total angular momentum quantum number is

$$P_{e,v,J} = e^{-\frac{(E_{e,v,J}-E_{e,v,J=0})}{kT_{\text{rot}}}} e^{-\frac{(E_{e,v,J=0}-E_{e,v=0,J=0})}{kT_{\text{vib}}}} e^{-\frac{E_{e,v=0,J=0}}{kT_{\text{ele}}}} \quad (1)$$

in which the temperature dependence is split into three exponentials with exponents relating to the rotational, vibrational and electronic state temperatures respectively. The first term is a function of the rotational temperature, T_{rot}, and pure rotational energy, $(E_{e,v,J} - E_{e,v,J=0})$, the second the vibrational temperature, T_{vib}, and pure vibrational energy, $(E_{e,v,J=0} - E_{e,v=0,J=0})$, and the third the electronic state temperature, T_{ele}, and the pure electronic state energy, $E_{e,v=0,J=0}$.

Einstein A-values, here provided by Duo, along with the populations are used to generate transition intensities, $I_{e'',v'',e',v','}$. ExoCross then uses line positions, also from Duo, and generates Gaussians with a width of the spectrometer's instrument function, $w \approx 1.5$ Å ($\approx 0.6\,\text{cm}^{-1}$), and an area of the calculated transition intensity, $I_{e'',v'',e',v','}$. These individual Gaussians are summed, giving the emitted intensity at a given energy.

In taking different rotational, vibrational and electronic temperatures ExoCross allows us to more accurately fit non-LTE spectra. This procedure is useful in the case where LTE has not been reached by the molecule producing the spectra. In such an instance the different spacing between electronic, vibrational, and rotational energy levels means that they adapt to changing temperatures and plasma conditions at different rates. In the cases discussed here the necessary time to reach equilibrium is too long and the plasma density too low for LTE conditions.

The ExoCross calculation is repeated for rotational and vibrational temperatures varying independently from 500 to 10000 K. For each combination of vibrational and rotational temperatures a program 'diffspec' is used to integrate the area under both curves, the overlap, and the area between the curves, the difference. The metric minimized to find the best fit temperature is the difference divided by the overlap. The theoretical and experimental spectra are both normalized, in the first instance, to have Q-branch peak values of 1.0. A multiplicative factor is then required to allow the peak values to differ. The experimental spectrum also contains a background which must be removed before matching to the theoretical spectrum, which necessitates a threshold. Also a higher weighting should be placed on fitting to the more intense parts of the experimental spectra which have the smallest experimental uncertainties in measurement. To this end, there are three inputs which adjust the intensity to control the nature of the fitting: factors, background thresholds and weight. The factors are applied to the synthetic spectrum by multiplying the intensity by a series of factors, here 0.8–1.2 in steps of 0.05. This allows the normalized spectra of arbitrary intensities to have different maximum values with respect to one another. For each factor thresholds are applied to the experimental spectra, moving each one up or down by an amount which varies from 0.0 to 0.1 in steps of 0.01. This allows the background in the experimental spectrum to be accounted for even if it differs between spectra recorded in different discharges. The last control input is a weight,

Table 5. Section of the states file produced by Duo for BeH with column format explanation.

1	2	3	4	5	6	7	8	9	10	11
n	E	m	J	$P_{+/-}$	$P_{e/f}$	State	v	Λ	Σ	Ω
1	0	16	0.5	+	e	X2Sigma+	0	0	0.5	0.5
2	1986.305 446	16	0.5	+	e	X2Sigma+	1	0	0.5	0.5
3	3896.800 417	16	0.5	+	e	X2Sigma+	2	0	0.5	0.5
4	5729.271 094	16	0.5	+	e	X2Sigma+	3	0	0.5	0.5
5	7480.454 45	16	0.5	+	e	X2Sigma+	4	0	0.5	0.5
6	9145.422 113	16	0.5	+	e	X2Sigma+	5	0	0.5	0.5
7	10 716.677 675	16	0.5	+	e	X2Sigma+	6	0	0.5	0.5
8	12 182.709 789	16	0.5	+	e	X2Sigma+	7	0	0.5	0.5
9	13 525.549 349	16	0.5	+	e	X2Sigma+	8	0	0.5	0.5
10	14 716.276 652	16	0.5	+	e	X2Sigma+	9	0	0.5	0.5

Column	Notation	
1	n	Rovibronic counting number
2	E	Energy of rovibronic state relative to ground state (cm^{-1})
3	m	multiplicity, including nuclear spin degeneracy
4	J	Total angular momentum quantum number
5	$P_{+/-}$	Parity in $+/-$ notation
6	$P_{e/f}$	Parity in e/f notation
7	State	Electronic state
8	v	Vibrational quantum number
9	Λ	Projection of electronic orbital angular momentum quantum number
10	Σ	Projection of electron spin angular momentum quantum number
11	Ω	Projection of total electronic angular momentum quantum number

Table 6. Section of the trans file produced by Duo for BeH with column format explanation.

1	2	3	4
n''	n'	A	$\tilde{\nu}$
71	1	4.58E-10	16 933.174 781
89	1	5.63E-02	38 037.683 830
65	1	8.17E-11	16 699.528 089
58	1	2.58E-07	12 198.141 744
95	1	6.48E-03	38 492.659 618
83	1	1.95E-01	32 206.945 906
51	1	1.12E-09	20.326 390

Column	Notation	
1	n'	Initial rovibronic state number, see table 5
2	n''	Final rovibronic state number, see table 5
3	A	Eisenstein A-coefficient (s^{-1})
4	$\tilde{\nu}$	Transition wavenumber (cm^{-1})

allowing a higher weighting to be given to the higher intensity portions of the spectrum for both the difference and the overlap. This is achieved by weighting each intensity by a power, here a weighting of 2.0 is used, the area effectively being squared. This ensures a sensible relation between the uncertainty in an intensity measurement and the magnitude of that intensity. There are also input parameters which are set to ignore certain, polluted, regions of the spectra from the area summation.

4.1. BeH analysis

Figures 4 and 6 compare experimental BeH spectra with the theoretical spectra generated by the computational methods described in section 2. An invasive H-atom line, H_{β}, is marked in figure 4; this region was excluded from the temperature fitting procedure in diffspec as described above. The best fit temperature for this spectra has $T_{\mathrm{rot}} = (540 \pm 70)$ K and $T_{\mathrm{vib}} = (3300 \pm 300)$ K meaning that the emission is from a

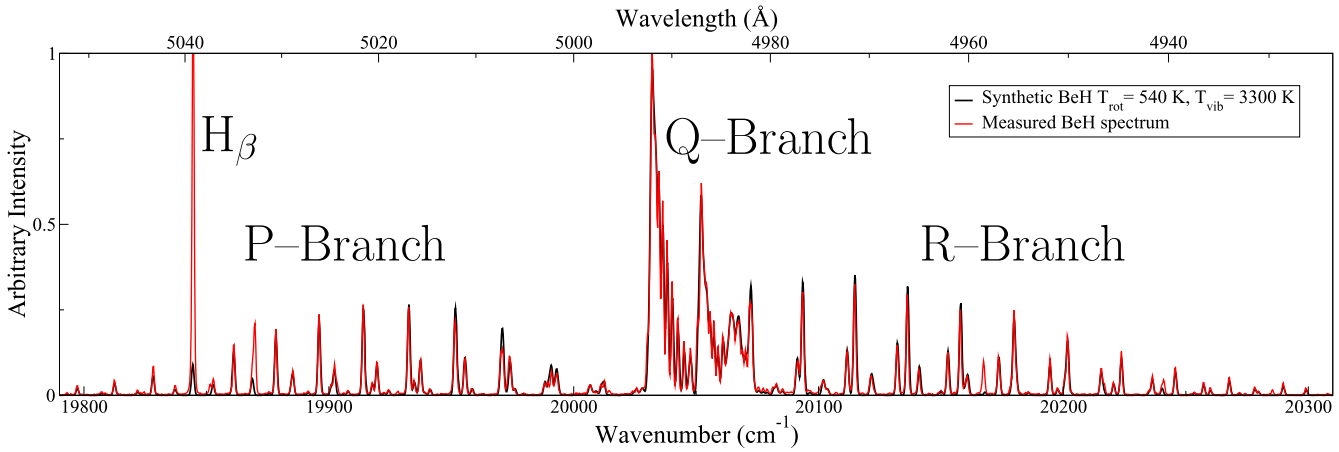

Figure 4. Measured BeH spectrum, shown in red, was recorded with a high resolution visible spectrometer from a hydrogen doped lamp with a beryllium target. Assigned synthetic spectrum of BeH, in black, is generated with $T_{\mathrm{rot}} = 540$ K and $T_{\mathrm{vib}} = 3300$ K using our BeH line list.

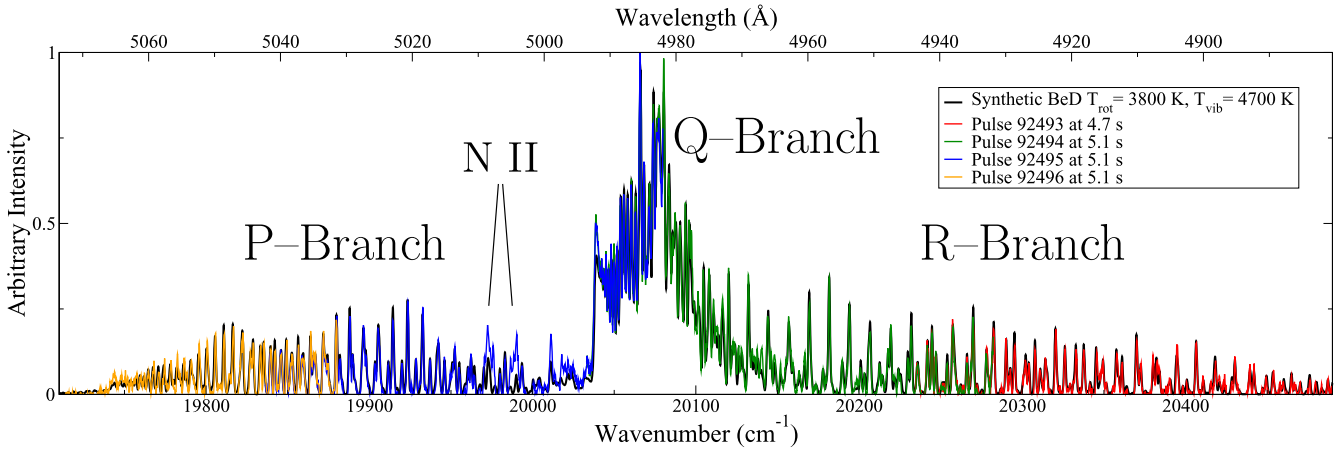

Figure 5. Measured BeD spectra, in red, green, blue and orange lines with pulse numbers and times in the legend, were recorded with a high resolution spectrometer, $T_e \approx 30$ eV and $n_e \approx 10^{-18}$ m^{-3}. Assigned synthetic spectrum, in black, is generated with $T_{\mathrm{rot}} = 3800$ K and $T_{\mathrm{vib}} = 4700$ K using our BeD line list.

non-LTE plasma. The fitting metric for this combination of rotational and vibrational temperatures = 0.208. Uncertainties were obtained from the greatest variation in temperature within 10% increase of the metric. The extreme difference between the vibrational and rotational temperatures is a product of the method by which the spectrum was produced. The need for a much higher vibrational temperature is illustrated by the presence of the 1–1 vibrational band head around 20050 cm^{-1} in figure 4 which is absent for $T_{\mathrm{vib}} = T_{\mathrm{rot}} = 540$ K. This would be the spectrum of BeH in LTE at 540 K and it clearly shows all of the primary peaks, that is all the transitions from fundamental vibrational quanta $v' = 0$ to $v'' = 0$. What is missing are all the lower intensity peaks which are produced by transitions from higher vibrational states. When the vibrational temperature is brought up to the best fit temperature of 3300 K the lower intensity, higher vibrational, components of the spectrum are brought sharply into alignment with the experimentally observed spectrum.

The degree of matching to the experimental spectra is highlighted by the close-up view of the R-branch shown in figure 6. The transition assignment labels here show that the vibrational quanta $v' = 0$ to $v'' = 0$ transitions are more intense and those of higher vibrational quanta are lower in intensity. The assignments show in order left to right: v' = upper state vibrational quantum number, N' = upper state nuclear rotational quantum number, v'' = lower state vibrational quantum number, N'' = lower state nuclear rotational quantum number. The heights of the transition lines in this figure are proportional to the A-values of the transitions not to the transition intensities. Hence, these lines do not necessarily correspond one to one to the height of the peaks in the synthetic spectrum which are dependent on temperature based populations, see equation (1), as well as A-values.

4.2. BeD analysis

A match was made between the experimental BeD spectrum from JET and a theoretical spectrum by varying the vibrational and rotational temperatures. Figure 5 shows an assigned synthetic spectrum generated at $T_{\mathrm{rot}} = (3800 \pm 700)$ K and $T_{\mathrm{vib}} = (4700 \pm 800)$ K using our BeD line list. The fitting metric for this combination of rotational and vibrational

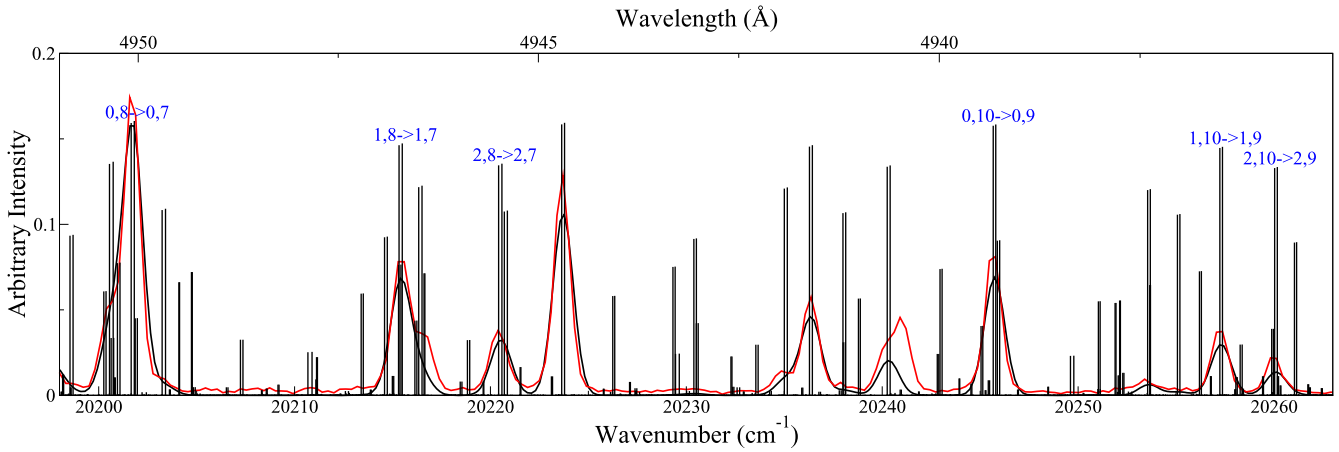

Figure 6. Magnified R-branch synthetic BeH A–X spectrum as in figure 4, generated at $T_{rot} = 540$ K and $T_{vib} = 3300$ K. Measured BeH spectrum is shown in red and transition assignments with drop lines in black. Assignments show in order left to right: v'' = upper state vibrational quantum number, N'' = upper state nuclear rotational quantum number, v' = lower state vibrational quantum number, N' = lower state nuclear rotational quantum number.

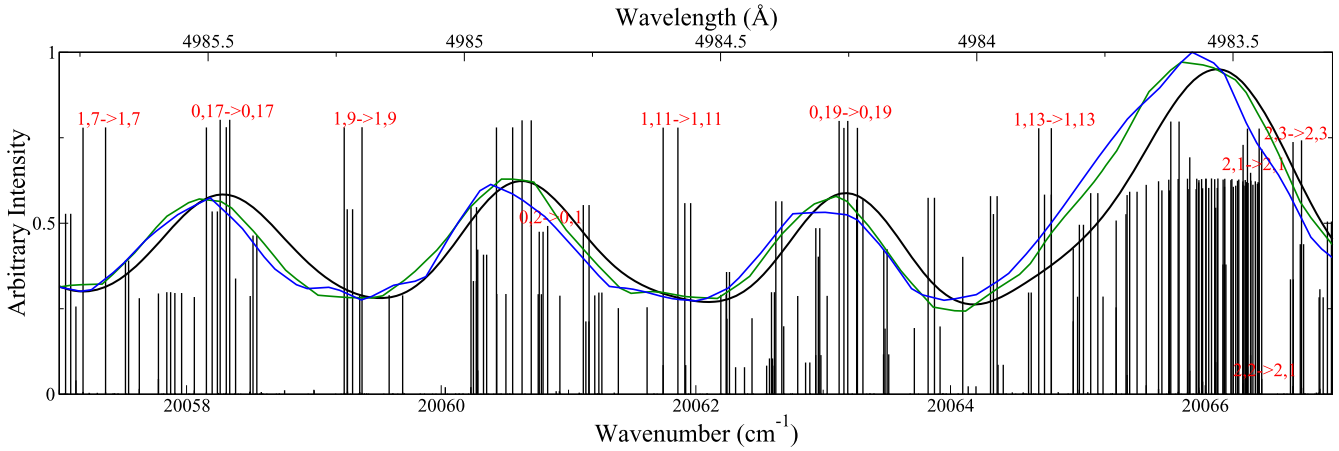

Figure 7. Magnified Q-Branch synthetic BeD A–X spectra as in figure 5, generated at $T_{rot} = 3800$ K and $T_{vib} = 4700$ K. Transition assignments with drop lines in black and high resolution JET measured spectra in green and blue. Assignments show in order left to right: v'' = upper state vibrational quantum number, N'' = upper state nuclear rotational quantum number, v' = lower state vibrational quantum number, N' = lower state nuclear rotational quantum number.

temperatures = 0.254. Uncertainties were obtained from the greatest variation in temperature within 10% increase of the metric. This combination of experimental BeD spectra has also been fitted assuming LTE ($T_{rot} = T_{vib}$). This gave a result of $T_{rot} = T_{vib} = (4300 \pm 600)$ K with the fitting metric = 0.274. This temperature fitting was also repeated while excluding the under-fitted vibrational 0–0 band head for both LTE and non-LTE assumptions. This gave a result of $T_{rot} = T_{vib} = (4400 \pm 600)$ K for LTE with the fitting metric = 0.252 and $T_{rot} = (4100 \pm 700)$ K and $T_{vib} = (4700 \pm 800)$ K for non-LTE with the fitting metric = 0.236.

Measured BeD spectra were recorded during the limiter phase of discharges 92 493–92 496. The vibrational and rotational temperatures fitted to the joined spectrum for BeD are much closer than in the BeH spectrum above, meaning the plasma conditions were much closer to LTE. There are four features, around ≈20 000 cm^{-1} in the JET spectra which are not reproduced in the synthetic spectrum. These are invasive features from other species, two being impurity lines of remaining nitrogen in the plasma.

Figure 7 shows a close-up section of the Q-branch with black drop lines at every transition energy in the region. This figure demonstrates the high degree of accuracy present across the range of these calculations.

The paper by Duxbury *et al* (1998) shows fittings for several molecular features in JET spectra including a BeD spectrum of the A to X transition. They fit a synthetic spectrum to an observed spectrum, which is generated using molecular constants. These constants are only valid for each isotopologue individually. By visual comparison, our work shows an improvement in line positions and in intensities.

4.3. BeT predictions

Figure 8 shows a predicted synthetic spectrum of the A–X transition of BeT. The rotational and vibrational temperatures used to generate this spectrum are those found for BeD in the

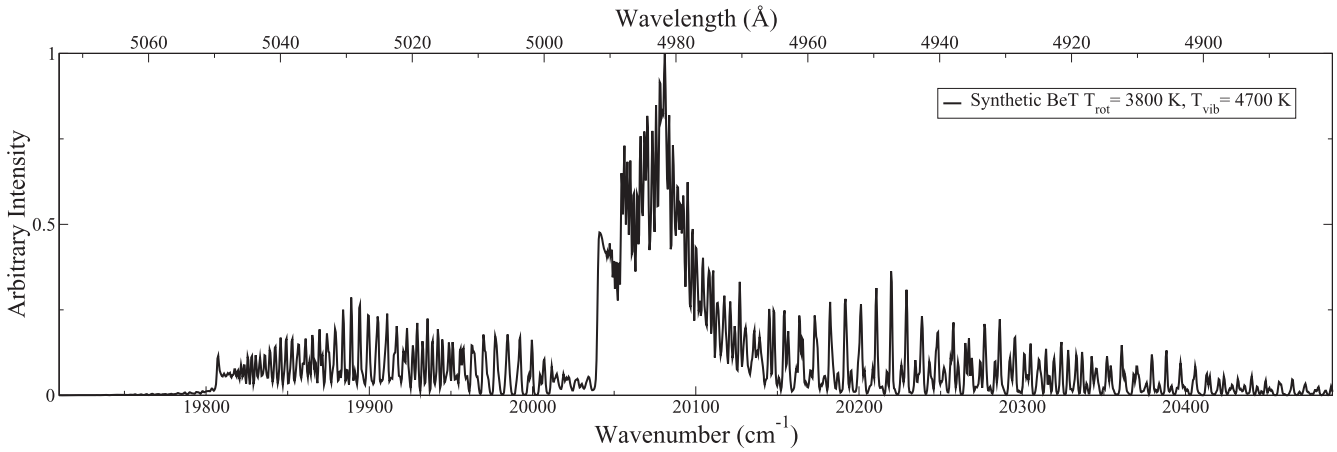

Figure 8. Predicted synthetic spectrum of BeT A–X calculated at $T_{\rm rot} = 3800$ K and $T_{\rm vib} = 4700$ K.

JET discharges discussed before. This is the BeT rovibronic spectrum expected to be observed in JET during a pure tritium campaign in discharges similar to those in which the BeD spectra were observed. The degree of accuracy in the results for BeT, and any isotopologue of BeH, is expected to be as seen in figure 6 for BeD. This will be compared with future JET and ITER spectra with their D/T fuel mix.

5. Conclusions

We construct line lists for the species BeH, BeD and BeT by using a mixture of fits to empirical energy levels to obtain PECs, coupling terms and beyond Born–Oppenheimer corrections. We conclude from a comparison of a synthetic spectrum fitted to experimental BeH and BeD spectra that our line lists reproduce the spectra of BeH, BeD and BeT to good accuracy. This accuracy is shown in figures 6 and 7 and is assured for BeT by the isotopologue consistency of our model. The comparisons show discrepancies in the intensities, for example, in the case of the BeD spectrum mostly seen in the Q-branch $v = 0$–0 band head. In the synthetic spectrum, the rotational temperature is too high to match this band head, which increases in relative intensity with decreasing rotational temperature. There are two possible explanations for this issue: firstly the theoretical model uses a statistical population model, which assumes a thermal equilibrium; the second possibility is that the line of sight for the experimental spectrum passes through different temperature regions, all radiating and giving a cumulative result. The first of these issues will be addressed in a future publication (Darby-Lewis and Tennyson 2018) by introducing a full collisional-radiative population model utilizing vibrationally averaged R-matrix results from the calculations of Darby-Lewis *et al* (2017) extended over bond lengths. The issue with the line of sight can be solved with a line of sight integration calculation applied to the results of the full population model. A possible third explanation is self absorption but given the very thin (less than 1 cm) layer of plasma containing BeD in the limiter region observed this is not thought to be able to significantly contribute to the effect seen on the 0–0 vibrational band head, this assumption will be tested in future work when we include a full collisional-radiative population model.

Finally, in a comparison with the previous work on BeD spectra modeling at JET by Duxbury *et al* (1998), we conclude that a more accurate and more comprehensive model has been achieved for two reasons. Firstly, the accuracy of the transition frequency fitting is much increased in our work. Secondly, our model is built using a single dataset derived from all the experimental transition data to model the three isotopologues. Not only does this improve the accuracy of the model, but it also enables accurate predictions to be made for the sparsely observed BeT isotopologue.

Acknowledgments

We would like to thank Dr Marie Gorman and Grace Eickmann for sharing their work on MARVEL for BeH, BeD and BeT with us. We would like to thank the Engineering and Physical Sciences Research Council (EPSRC) for studentship (EP/M507970/1) and the Culham Centre for Fusion Energy (CCFE) for funding. This work was carried out within the framework of the EUROfusion Consortium and has received funding from the Euratom research and training programme 2014-2018 under grant agreement No. 633053 and from the RCUK Energy Programme [Grant number EP/P012450/1]. The views and opinions expressed herein do not necessarily reflect those of the European Commission.

ORCID iDs

J Tennyson https://orcid.org/0000-0002-4994-5238
S Brezinsek https://orcid.org/0000-0002-7213-3326

References

Bernath P F 2005 *Spectra of Atoms and Molecules* 2nd edn (Oxford: Oxford University Press)

Björkas C, Borodin D, Kirschner A, Janev R K, Nishijima D, Doerner R and Nordlund K 2013 *J. Nucl. Mater.* **438** S276–9
Borodin D *et al* 2011 *Phys. Scr.* **T145** 014008
Brezinsek S, Pospieszczyk A, Sergienko G, Mertens P and Samm U 2008 *Plasma Fusion Res.* **3** S1041
Brezinsek S, Stamp M F, Nishijima D, Borodin D, Devaux S, Krieger K, Marsen S, O'Mullane M, Bjoerkas C and Kirschner A 2014 *Nucl. Fusion* **54** 103001
Colin R, Dreze C and Steinhauer M 1983 *Can. J. Phys.* **61** 641–55
Darby-Lewis D, Masin Z and Tennyson J 2017 *J. Phys. B: At. Mol. Opt. Phys.* **50** 175201
Darby-Lewis D and Tennyson J 2018 *J. Phys. B: At. Mol. Opt. Phys.* in preparation
Dattani N S 2015 *J. Mol. Spectrosc.* **311** 76–83
De Greef D and Colin R 1974 *J. Mol. Spectrosc.* **53** 455–65
Duxbury G, Stamp M F and Summers H P 1998 *Plasma Phys. Control. Fusion* **40** 361
Focsa C, Bernath P F, Mitzner R and Colin R 1998 *J. Mol. Spectrosc.* **192** 348–58
Furtenbacher T and Császár A G 2012 *J. Quant. Spectrosc. Radiat. Transfer* **113** 929–35
Furtenbacher T, Császár A G and Tennyson J 2007 *J. Mol. Spectrosc.* **245** 115–25
Hornkohl J O, Parigger C and Lewis J W L 1991 *J. Quant. Spectrosc. Radiat. Transfer* **46** 405–11
Huber K P and Herzberg G 1979 *Molecular Spectra and Molecular Structure IV. Constants of Diatomic Molecules* (New York: Van Nostrand-Reinhold)
Koput J 2011 *J. Chem. Phys.* **135** 244308
Lasa A, Borodin D, Canik J M, Klepper C C, Groth M, Kirschner A, Airila M, Borodkina I and Ding R 2018 *Nucl. Fusion* **58** 016046
Le Roy R J 2017 *J. Quant. Spectrosc. Radiat. Transfer* **186** 167–78
Le Roy R J, Appadoo D R T, Colin R and Bernath P F 2006 *J. Mol. Spectrosc.* **236** 178–88
Le Roy R J, Haugen C C, Tao J and Li H 2011 *Mol. Phys.* **109** 435–46
McGuire S D, Tibère-Inglesse A C and Laux C O 2016 *J. Phys. D: Appl. Phys.* **49** 485502
Parigger C G, Woods A C, Surmick D M, Gautam G, Witte M J and Hornkohl J O 2015 *Spectrochim. Acta* B **107** 132–8
Pitarch-Ruiz J, Sanchez-Marin J, Velasco A M and Martin I 2008 *J. Chem. Phys.* **129** 054310
Shayesteh A, Tereszchuk K, Bernath P F and Colin R 2003 *J. Chem. Phys.* **118** 1158–61
Tennyson J, Hill C and Yurchenko S N 2013 *6th Int. Conf. on Atomic and Molecular Data and their Applications ICAMDATA-2012* (*AIP Conference Proceedings* vol 1545) (New York: AIP) pp 186–95
Tennyson J and Yurchenko S N 2012 *Mon. Not. R. Astron. Soc.* **425** 21–33
Tennyson J *et al* 2016 *J. Mol. Spectrosc.* **327** 73–94
Yadin B, Vaness T, Conti P, Hill C, Yurchenko S N and Tennyson J 2012 *Mon. Not. R. Astron. Soc.* **425** 34–43
Yurchenko S N, Al-Refaie A F and Tennyson J 2018 *Astron. Astrophys.* **614** A131
Yurchenko S N, Lodi L, Tennyson J and Stolyarov A V 2016 *Comput. Phys. Commun.* **202** 262–75